PROCESS OPTIMIZATION FOR WELDING SINGLE-CRYSTAL NICKEL-BASED SUPERALLOYS

J. M. Vitek
S. S. Babu
S. A. David
Oak Ridge National Laboratory
P. O. Box 2008
Oak Ridge, Tennessee 37831-6096

PROCESS OPTIMIZATION FOR WELDING SINGLE-CRYSTAL NICKEL-BASED SUPERALLOYS

J. M. Vitek
S. S. Babu
S. A. David
Oak Ridge National Laboratory
P. O. Box 2008
Oak Ridge, Tennessee 37831-6096

Abstract

Welding of nickel-based single-crystal superalloys typically results in the formation of stray grains, which are newly nucleated grains with crystallographic orientations different from that of the base metal. Consequently, the single-crystal nature of the alloy is lost. In earlier work, the mechanism of stray-grain formation during welding was identified as constitutional supercooling ahead of the advancing solidification front. In this project, the extent of stray-grain formation was analyzed as a function of welding conditions. A thermal model of the weld pool was integrated with a geometrical model that describes the preferred dendritic growth directions as a function of position in the weld pool, and a solidification model that describes the extent of stray-grain formation. The results provide critical information on the extent of stray-grain formation as a function of welding conditions. It was found that high weld speed and low weld power are optimal for maintaining the single-crystal structure of the base metal. When averaging over the entire weld pool, the effect of weld orientation on the extent of stray-grain formation is minimal, but orientation does have a strong effect on the microstructure at any given location on the weld pool. The model predictions agree quite well with experimental results.

Introduction

Advanced aircraft and land-based turbine engines utilize components made of single-crystal nickel-based superalloys in order to maximize performance and efficiency. Single crystals are used because they offer superior high-temperature properties, particularly creep strength. Such single-crystal components are expensive, and this is especially true in land-based turbine engines where they are significantly larger in size and represent significantly greater investment costs. Therefore, weld repair technologies are desirable for extending the life of these components, and

making the advanced turbine engines commercially viable. Welding is important for repairing damaged or worn parts as well as for refurbishing as-cast parts with defects in order to improve casting yields.

Nickel-based single-crystal turbine engine components consist primarily of a two-phase microstructure: an FCC gamma solid solution matrix phase and a uniform distribution of ordered gamma prime precipitates. The gamma matrix phase is a single crystal with no high-angle grain boundaries. The gamma prime precipitates are characteristically cuboidal in form and they are coherent with the matrix. Advanced single-crystal superalloys contain high volume fractions of gamma prime, typically in the range of 50 to 70 volume percent. The single-crystal nature of the microstructure, combined with the high volume fraction of gamma prime precipitates, provides the excellent high-temperature mechanical properties that are required.

Any successful welding process for single-crystal nickel-based superalloys should have the following characteristics:

- the welds must be crack-free;
- the welds should contain a high volume fraction of gamma prime precipitates in order to match the high strength of the base material;
- the welds should maintain the single-crystal nature of the base material in order to maximize the elevated-temperature creep properties.

Unfortunately, current welding procedures cannot meet these requirements. When filler metals with high volume fractions of gamma prime are used, weld cracking is common and often can be severe[1]. Fusion welds are also characterized by an abundance of stray grains, which are new grains that are formed during solidification. These stray grains have many different crystallographic orientations so that the single-crystal nature of the base material is lost. In addition, the high-angle grain boundaries that exist in conjunction with the stray grains are weak links in the microstructure and act as preferred crack propagation paths. An example of an autogenous electron beam weld made on alloy PWA1480 is shown in Figure 1 and all of these weld deficiencies are clearly visible. The extent of cracking is strongly dependent upon the volume fraction of gamma prime. Thus, crack-free fusion welds can be made with low gamma-prime-fraction filler metals, while high gamma-prime-fraction filler metals lead to cracking in welds. This is shown in Figure 2. Therefore, existing weld technologies must use inferior filler metals with low gamma prime volume fractions (or no gamma prime) in order to produce crack-free welds. Furthermore, the single-crystal microstructure is totally absent in the final

[1] This paper will focus on fusion welding techniques. Other joining methods, such as transient liquid phase bonding, may yield crack-free welds with higher gamma prime contents but those welds are still limited with regard to high-temperature properties, single-crystal microstructure, and phase stability.

weldments. Consequently, welded parts have severely compromised properties, and welding must be limited to sections that experience minimal loads.

A U.S. Department of Energy program was launched at Oak Ridge National Laboratory in 2001 to investigate the potential for producing crack-free welds that maintained a high volume percent of gamma prime as well as the single-crystal base metal microstructure. The objectives of this program were presented at the 5th International EPRI Conference on Welding and Repair Technology for Power Plants in 2002 (1). As this program nears completion, significant progress has been made in terms of understanding the mechanism of stray-grain formation and its consequences. Elimination of stray grains would maintain the single-crystal microstructure and would avoid the formation of high-angle grain boundaries and the cracking associated with them. This paper describes the results of this program and will show that crack-free single-crystal welds with high gamma prime volume fractions may be obtainable in the near future. While the paper focuses on autogenous welds, the results with regard to optimizing weld conditions to avoid stray-grain formation should be applicable to filler metal welds as well.

Experimental Work

Experimental autogenous welds were made on 0.8 mm-thick sheets made from a single-crystal slab of commercial alloy Rene N5. The alloy composition was (in wt %): Ni-7.11Cr- 7.32Co-6.25Al- 6.38Ta- 4.83W- 2.88Re-1.41Mo-0.15Hf-0.053C. The welds were full-penetration or nearly full-penetration laser welds. The welds were made parallel to the slab growth direction, on a surface perpendicular to the original slab surface. The crystallographic orientation of the sheet and weld direction were determined by Laue X-ray diffraction. The sheet normal direction was [-0.925, -0.376, 0.051] and the welding direction was [0.141, 0.217, -0.966]. The sheet normal deviated from the [-1, 0, 0] direction by 15°, and the weld direction deviated from [0,0,-1] by 22°. It is important to note that the weld orientation was not along an axis of symmetry, so that the weld centerline was also not a plane of crystallographic symmetry. This condition led to asymmetrical weld microstructures, as shown later. A range of conditions (power and speed) was used. Only representative results will be presented here. Further details may be found elsewhere (2). The as-welded microstructures were evaluated by optical microscopy. In addition, the grain structure of the laser welds was analyzed by Orientation Imaging Microscopy (OIM) to clearly reveal the presence of stray grains and associated high-angle grain boundaries.

A low-speed, low-power weld is shown in Figure 3 and a high-speed, high-power weld is shown in Figure 4. Several features are readily noticed. First, the low-speed, low-power weld is crack-free, while the high-speed, high-power weld shows cracking. Second, the cracks, when present, are clearly asymmetrically distributed. Third, stray grains are visible in both welds, but the extent of stray-grain formation is minimal in the low-speed, low-power weld and it is much more extensive in the high-speed, high-power weld. Fourth, as was the case for the cracking, the stray-grain formation is also asymmetrically distributed with respect to the weld centerline, with many more stray grains forming on the right side of the weld. Fifth, the stray grains did not form

near the fusion line, but rather they are concentrated near the weld centerline. Finally, the cracks formed along the high-angle grain boundaries of the stray grains. The same features were found for electron beam welds (3).

Results from OIM of the high-speed, high-power laser weld are shown in Figure 5. OIM is based on the crystallographic orientation of the sample and allows the variation in orientation across the weld, due to stray-grain formation, to be clearly demonstrated. The asymmetry in stray-grain formation is apparent, with few stray grains on the left side of the weld and extensive stray grains present on the right side. Further, stray-grain formation begins approximately halfway from the weld fusion line to the weld centerline. The crack (arrow in Figure 5) appears as a mottled streak and its path along the stray-grain high-angle grain boundary is evident.

Stray-grain Formation Mechanism

Two possible mechanisms for stray-grain formation have been proposed. One considers the fragmentation of growing dendrites due to vigorous fluid flow in the molten pool (4), as shown schematically in the top of Figure 6. The other is based on constitutional supercooling ahead of the advancing dendrite front, leading to nucleation and growth of new grains (5), shown schematically in the bottom of Figure 6. Several of the experimental observations in this study do not agree with predictions based on the fragmentation mechanism. Fragmentation theory predicts that stray-grain formation will be greater at the fusion line, where the cooling rates are highest (4). In addition, to a first order, fragmentation should be symmetrical with respect to the weld centerline, since fluid flow of the melt during welding is basically symmetrical. With further development of the theory, a dependence of fragmentation on orientation may evolve, but at present a dependence that would explain the observed asymmetry does not exist. Thus, while fragmentation appears to apply for stray-grain formation in casting, it may only be of secondary importance in welding. This is not unexpected, since the thermal conditions and fluid flow behavior are very different in welding and casting.

The constitutional supercooling mechanism for stray-grain formation has been examined quite extensively in recent years (6-8). It is based on the solute partitioning that takes place during solidification and is shown schematically in Figure 7. Rejection of solute ahead of the advancing solidification front leads to a zone of enriched liquid with a suppressed liquidus temperature compared to the overall alloy composition. If the thermal gradient is small, as shown in Figure 7, this liquid will be undercooled and nucleation and growth of new grains will be promoted. A simplified treatment of constitutional supercooling leads to the following condition for avoiding supercooling:

$$\frac{G}{V} > \frac{\Delta T}{D} \qquad (1)$$

where G is the thermal gradient, V is the growth velocity, ΔT is the solidification temperature range, and D is the diffusion coefficient in the liquid (5). More advanced treatments have been

developed recently and provide a more quantitative assessment of the extent of stray-grain formation (6-8). While many assumptions are included in the theoretical treatment of constitutional supercooling when applied to multi-component systems, such as the Rene N5 alloy used in this study, the theory leads to several specific predictions. With a detailed treatment of the nucleation of new grains, and their growth ahead of the advancing dendritic front, the following relationship was derived (8):

$$\frac{G^n}{V} = a\left\{\sqrt[3]{\frac{-4\pi N_0}{3\ln[1-\Phi]}}\frac{1}{n+1}\right\}^n \qquad (2)$$

where a and n are material constants, N_0 is the nucleation density, and Φ is the volume fraction of new, equiaxed grains (i.e, stray grains). A high value of Φ ($0.5 < \Phi < 1.0$) corresponds to basically complete stray-grain formation, while a small value of Φ ($\Phi \sim 0$) corresponds to no stray-grain formation. In the present analysis, the values for the three constants ($a = 1.25 \times 10^6$ $sK^{3.4}m^{-1}$, $n = 3.4$, and $N_0 = 2 \times 10^{15}$ m^{-3}) were the same as those used by Gäumann et al (8) for a similar nickel-based superalloy. One can rearrange Equation (2) to solve explicitly for the stray-grain fraction, obtaining:

$$\Phi = 1 - e^S \quad \text{where } S = \frac{-4\pi N_0}{3}\left(\frac{1}{(n+1)(G^n/aV)^{1/n}}\right)^3 = -2.56\times10^{19}\left(\frac{V}{G^{3.4}}\right)^{3/3.4} \qquad (3)$$

In the present analysis, the gradient and solidification front velocity vary across the weld pool. In addition, one must take into account the crystallographic orientation of the single crystal. In FCC materials such as the Rene N5 superalloy, there are six possible variants of the preferred dendritic growth directions ([100], [-100], [010], etc). Growth along any one of these base-metal directions would result in preservation of the single-crystal nature of the sample. At any given location, one must consider the thermal gradient and growth velocity along the six <100> variants. The active dendrite growth direction at any given location is the one corresponding to the minimum growth velocity, which corresponds to the minimum dendrite-tip undercooling (9). When such an analysis was performed, the results were found to be perfectly consistent with the experimental findings (10). It was found that Φ was a minimum at the weld fusion line and increased as the weld centerline was approached, in agreement with the experimental results that showed stray grains near the centerline (Figure 5). Taking into account the actual weld sample crystallographic orientation, it was found that Φ was asymmetrical with respect to the weld centerline, and it was significantly larger on the right side of the pool, where significantly more stray grains were observed. Based on these results, it was concluded that the constitutional supercooling mechanism correctly describes stray-grain formation tendencies in welds. This analysis was then used to evaluate the effect of weld conditions on stray-grain formation, as described in detail in the next section.

Effect of Weld Conditions on Stray-grain Formation – Modeling Results

Equation (3) was used to evaluate Φ as a function of weld speed, weld power, and weld sample crystallographic orientation. A simple 3D Rosenthal solution was used to describe the shape of the weld pool as a function of speed and power (11). While more accurate models for calculating the weld pool shape are available, the simple solution was used because it allowed for an easy evaluation of the entire weld pool surface, due to the inherent symmetry of the solution. Its simplicity made the calculations less demanding in terms of computational power, so that a wide range of conditions could be studied. Two different analyses were made. In the first, an overall average value of Φ (Φ_{AV}) was determined by taking the area-weighted average of Φ over the entire weld pool. In the second, the variation of Φ as a function of position in the weld pool was examined. The results for Φ_{AV} are presented in Figures 8 through 10. Figure 8 plots Φ_{AV} versus weld speed for a single orientation and three weld powers. Figure 9 shows Φ_{AV} versus weld power for one orientation and three weld speeds. Figure 10 shows Φ_{AV} for a fixed weld speed and power but seven different crystallographic orientations.

The results in Figure 8 show that Φ_{AV} decreases as the weld speed increases. This was found to be true in general, with only a few exceptions (10). At first this result appears to violate the simple analysis of constitutional supercooling, as expressed in Equation (1). In that equation, if all other variables are held constant (G, ΔT, D), then increasing velocity leads to a failure of the condition that must be met to avoid stray-grain formation. However, as the velocity increases, the gradient also increases. A steep gradient helps to avoid stray grains, as described in Equation (1). In fact, the more detailed expressions shown in Equations (2) and (3) show that changes in gradient are far more important than changes in velocity, since the gradient is raised to the 3.4 power.

Figure 9 shows that as the power increases, Φ also increases, so that the stray-grain formation tendencies increase. This is a direct consequence of the lower thermal gradients found at higher powers. In the experimental results, high-speed, high-power welds showed more extensive stray-grain formation (and cracking), which fits with the theoretical calculations. The change from low to high power has a greater impact that the concurrent change from low to high speed.

Figure 10 shows the effect of weld orientation on Φ_{AV}. It can be seen that the influence of orientation on Φ_{AV} is minimal. As shown later, while orientation does have an influence on the value of Φ at any given location, in general, the stray-grain-free regions balance against the stray-grain-prone regions, so that the average remains more or less independent of orientation.

An overall map of Φ_{AV} versus weld speed and power is shown in Figure 11. Contour lines have been fitted to the calculated conditions, representing over 20 different combinations of weld speed and power, covering the range of speeds from 0.0042 to 0.42 m/s and powers from 420 to 4000 W. The map in Figure 11 clearly identifies the preferred operating conditions. Low values of Φ_{AV}, corresponding to minimal tendencies to form stray grains during welding, are found at low powers and high weld speeds.

Finally, Figure 12 shows a 3D diagram of the weld pool for three different weld conditions. In Figure 12a, a low-speed, low-power weld made in a symmetric orientation ([100] weld direction on an (001) plane) is shown. Figure 12b shows a weld made at the same speed and power, but made in an asymmetrical orientation ([310] direction on (1 -3 7) plane). Figure 12c shows a high-speed, low-power weld made on the same symmetric orientation, as in Figure 12a. Calculations were made over the entire weld pool surface (represented by data points in the figures) and the values of Φ at any given location were used to color code the data points. Blue represents Φ = 0 and red corresponds to Φ = 1. Values between 0 and 1 correspond to colors between blue and red, respectively. The figures show many interesting features. Figure 12a shows that the distribution of Φ around the entire weld pool is symmetrical with respect to the centerline, as expected for a symmetrical crystallographic orientation. In addition, low values of Φ were found near the weld fusion line, while higher values were found toward the centerline. The values of Φ can be correlated directly to the degree to which the active dendrite growth variant (among the six possible choices) is aligned with the solidification front normal. Thus, in Figure 12a, Φ reaches a maximum between the fusion line and centerline, and at the centerline it drops somewhat. This is because at the centerline, the active dendrite growth direction is [100], and is perfectly aligned with the solidification front normal at the centerline.

Figure 12b represents an asymmetrical weld orientation and this is reflected by the asymmetry in the distribution of Φ around the weld pool. In this figure, one side of the weld pool maintains relatively low values of Φ throughout, while the other side has a large zone with high values of Φ (large zone of nearly pure-red points). Finally, Figure 12c shows the case for a high-speed weld made in a symmetrical orientation. It can be seen that over a large portion of the weld pool, the value of Φ is quite low, as indicated by the blue color of the data points. At high speeds, the weld pool shape is elongated and the thermal gradients are larger. Both of these effects lead to lower values of Φ. However, near the centerline, Φ becomes quite large. In fact the data points are nearly pure red, indicating a value of $\Phi \sim 1$. This is higher than found in Figures 12a or 12b, but is limited to a relatively small area fraction of the total weld pool. Near the centerline, the weld pool surface curvature is significant. Consequently, the high values of Φ are found near the centerline, but at the exact centerline the value of Φ drops to near zero (not shown in figure) as a result of the perfect alignment between the dendrite growth direction and the solidification front normal.

Outstanding Issues

The present work considered the influence of welding conditions on the stray-grain formation tendencies in single-crystal welds. Optimum welding conditions were identified and it was shown that stray-grain free, crack-free welds with high gamma prime volume fractions may be obtained. However, several issues remain to be addressed before successful welds can be obtained routinely and commercial implementation of a weld repair technology can be achieved.

Figure 12 shows that the propensity to form stray grains varies across the weld pool. There are certain “hot spots” in the welds where stray grains are more likely to form, and these locations

vary with weld conditions and the crystallographic orientation of the weld. As shown in Figures 1 and 2, the high-angle grain boundaries produced by stray grains act as preferred locations for cracking. This is not surprising, since such boundaries are weak links in the microstructure. No adjustments in the alloy are made to strengthen these boundaries since single-crystal superalloys are designed to be free of high-angle grain boundaries. Thus, it is likely that stray-grain free areas can tolerate higher stresses that are generated during welding, but if stray grains are present, these same stresses may be beyond a critical level and cracks may develop. Therefore, it is necessary to integrate calculations of stray-grain formation behavior across the entire weld pool with calculations of the stresses that develop during welding, to determine how optimum weld conditions for avoiding stray-grain formation can be combined with optimum conditions for minimizing stresses during welding.

Even when stray grains are avoided, single-crystal welds will be characterized by distinct zones where the dendrite growth directions are different. This is a consequence of the fact that across the entire weld more than one of the six possible <100> dendrite growth variants will be active. Additional work is required to investigate the mechanical properties of microstructures that contain such dendrite zone boundaries. It must be determined if these boundaries have an influence on the strength of the weld. This is a question that has yet to be investigated.

Additional work in this DOE project, not reported here, has shown that commercial single-crystal nickel-based superalloys characteristically exhibit a ductility minimum at elevated temperatures (12). This behavior is likely to be associated with hot-cracking tendencies and may be related to the ductility dip phenomenon commonly found in polycrystalline alloys. In order to obtain crack-free welds, more work is needed to investigate the nature of this ductility minimum and the means by which this behavior can be eliminated, or at least minimized.

The as-welded microstructures are considerably finer than those in the base metal. It has been shown elsewhere (13) that, after laser welding, the gamma prime precipitate size is extremely fine, and moreover, the precipitates do not have the characteristic cuboidal morphology found in the base metal. Further work is required to determine the stability of the as-welded microstructure. The potential for coarsening of the microstructure must be assessed, and the impact that any morphological instability may have on mechanical properties must be established.

While the present work concentrated on autogenous welds, the results should apply equally well to filler metal welds. Filler metal alloy optimization is yet another possible means for reducing the stray-grain formation tendencies. It is well known that the solidification temperature range has a direct impact on the extent of constitutional supercooling. While the influence of ΔT on Φ is not clear in Equations (2) and (3), it's direct relationship to the constitutional supercooling condition is shown in the more simplified Equation (1). Reducing ΔT will decrease the critical value of G/V that is needed to avoid constitutional supercooling and the formation of new stray grains. This relationship has been verified qualitatively by comparing the ease with which stray-grain-free welds can be made for several different alloy types (14). In the current DOE program, potential modifications to standard single-crystal superalloy compositions that would reduce the

ΔT are being investigated. Such modified filler metal compositions may allow for improved welds without significantly altering the mechanical properties and phase stability of the weld metal. However, further work is required in order to assess the benefit of these changes and to determine the mechanical properties of welds made with such modified filler metals.

Summary and Conclusions

This paper reports on progress made in a DOE-sponsored project on weld repair of single-crystal, nickel-based superalloys. The aim of the project was to investigate the potential for producing stray-grain-free, crack-free, high gamma prime-content welds. Experimental results showed that stray-grain-free weld microstructures could be produced. It was found that without the formation of stray grains and associated high-angle grain boundaries, crack-free welds could also be achieved. Analysis of experimental welds indicated that the tendency to form stray grains can be described by calculations based on the constitutional supercooling mechanism. The optimum weld conditions for producing welds that maintain the single-crystal base metal structure and avoid the formation of stray grains were identified. Examination of the effects of weld speed, weld power, and crystallographic orientation showed that the combination of high speed and low power minimize the probability of forming stray grains. It was also shown that, when considering the average stray-grain formation tendency over the entire weld pool, the crystallographic orientation has very little influence. However, the probability of forming stray grains varies across the weld pool, and the tendency to form stray grains at any given location is strongly dependant upon orientation. Finally, remaining questions that must be addressed before the commercial implementation of a weld repair technology can be achieved were identified.

Acknowledgments

The authors would like to thank their industrial and university partners in this project (EPRI-RRAC, General Electric Corporation, Honeywell Aerospace Services, PCC Airfoils, Pratt & Whitney Corporation, Siemens-Westinghouse Corporation, and South Carolina Institute for Energy Studies) for providing helpful insight and guidance. In addition, the authors thank General Electric Corporation for providing the Rene N5 alloy and PCC Airfoils Corporation for performing the chemical analysis. This research was sponsored by the Office of Fossil Energy, U.S. Department of Energy, National Energy Technology Laboratory, and the Division of Materials Sciences and Engineering, U. S. Department of Energy, under Contract DE-AC05-00OR22725 with UT-Battelle, LLC.

References

1. J. Vitek, S. David, S. Babu, “Welding and Weld Repair of Single Crystal Gas Turbine Alloys,” paper GT10 in Conference Proceedings: EPRI-RRAC Fifth International Conference on Welding and Repair Technology for Power Plants, June 26-28, 2002, Point Clear, Alabama.

2. J-W. Park, S. S. Babu, J. M. Vitek, E. A. Kenik and S. A. David, "Stray Grain Formation in Single Crystal Ni-Base Superalloy Welds," *J Appl Phys* 2003, 94(6), 4203-4209.

3. J. M. Vitek, S. S. Babu, J-W. Park, and S. A. David, "Stray Grain Formation in Nickel-Base Superalloy Single-Crystal Welds," p 61-67 in *Solidification Processes and Microstructures: A symposium in Honor of Wilfried Kurz*, eds M. Rappaz, C. Beckermann and R. Trivedi, TMS, Warrendale, PA, 2004.

4. T. M. Pollock and W. H. Murphy, "The Breakdown of Single-Crystal Solidification in High Refractory Nickel-Base Alloys," *Metall Mater Trans A*, 1996, 27A, 1081-1094.

5. W. Kurz and D. J. Fisher, p 240 in *Fundamentals of Solidification*, Trans Tech Publications, Aedermannsdorf, Switzerland, 1984.

6. J. D. Hunt, "Steady State Columnar and Equiaxed Growth of Dendrites and Eutectics", *Mater Sci Eng*, 1984, 65, 75-83.

7. M. Gäumann, R. Trivedi and W. Kurz, "Nucleation Ahead of the Advancing Interface in Directional Solidification," *Mater Sci Eng*, 1997, A226-228, 763-769.

8. M. Gäumann, C. Bezençon, P. Canalis and W. Kurz, "Single-Crystal Laser Deposition of Superalloys: Processing-Microstructure Maps", *Acta Mater*, 2001, 49, 1051-1062.

9. M. Rappaz, S. A. David, J. M. Vitek and L. A. Boatner, "Development of Microstructures in Fe-15Ni-15Cr Single Crystal Electron Beam Welds," *Metall Trans A*, 1989, 20A, 1125-1138.

10. J. M. Vitek, "The Effect of Welding Conditions on Stray Grain Formation in Single Crystal Welds – Theoretical Analysis," submitted for publication in *Acta Materialia*, 2004 .

11. D. Rosenthal, "Mathematical Theory of Heat Distribution during Cutting and Welding," *Weld J*, 1941, 20(5), 220s-234s.

12. S. S. Babu, Oak Ridge National Laboratory, unpublished results, 2004.

13. S. S. Babu, S. A. David, J. M. Vitek, and M. K. Miller, "Atom-Probe Field Ion Microscopy Investigation of CMSX-4 Ni-Base Superalloy Laser Beam Welds," *J. de Physique IV, Colloq. C5, suppl. J. de Physique III*, 1996, 6, C5-253 - C5-258.

14. J. M. Vitek, S. S. Babu, S. A. David, and J-W. Park, "Microstructure Development in Single Crystal Welds," *Mater Sci Forum* 2003, 426-432, 4123-4128.

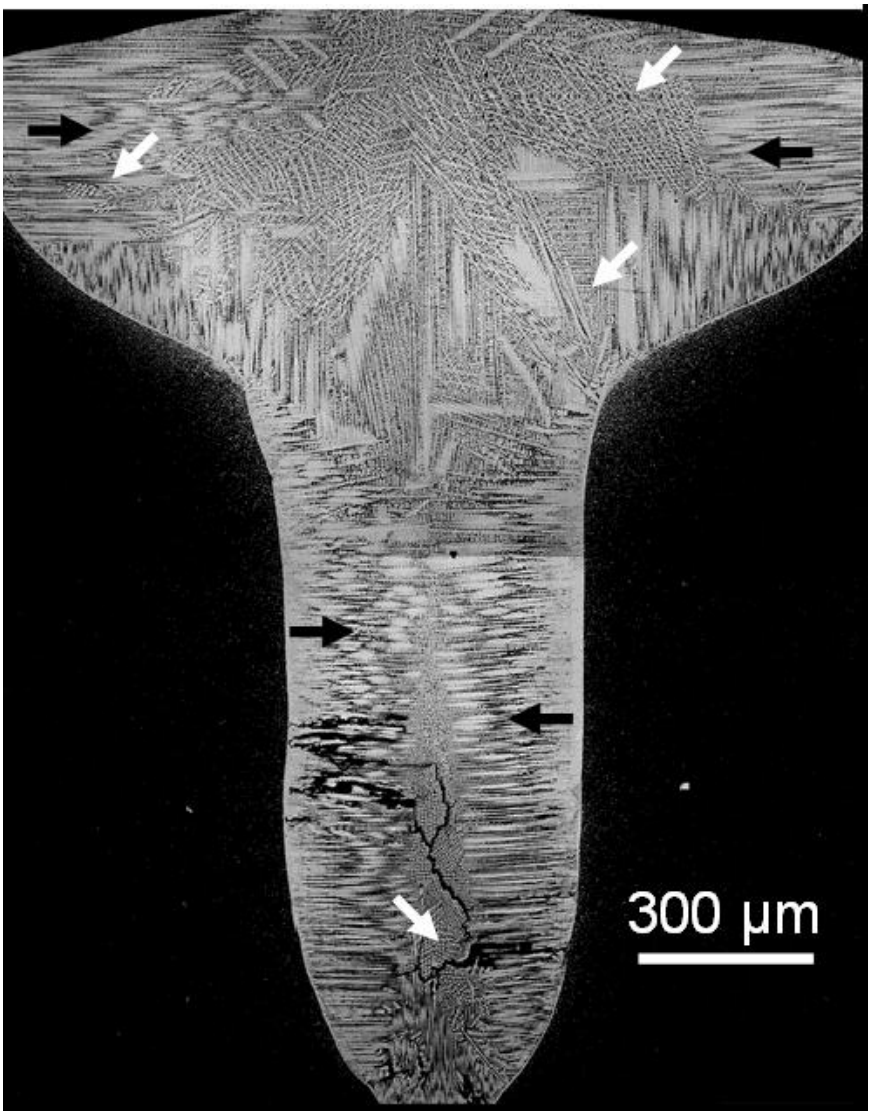

Figure 1: Cross-section of electron beam weld made along [100] direction and on (001) plane of commercial alloy PWA 1480, showing extensive stray-grain formation (white arrows) and crack formation. Some of the regions with epitaxial dendritic growth, that retain the base metal single-crystal orientation, are shown with black arrows pointing along dendrite growth direction.

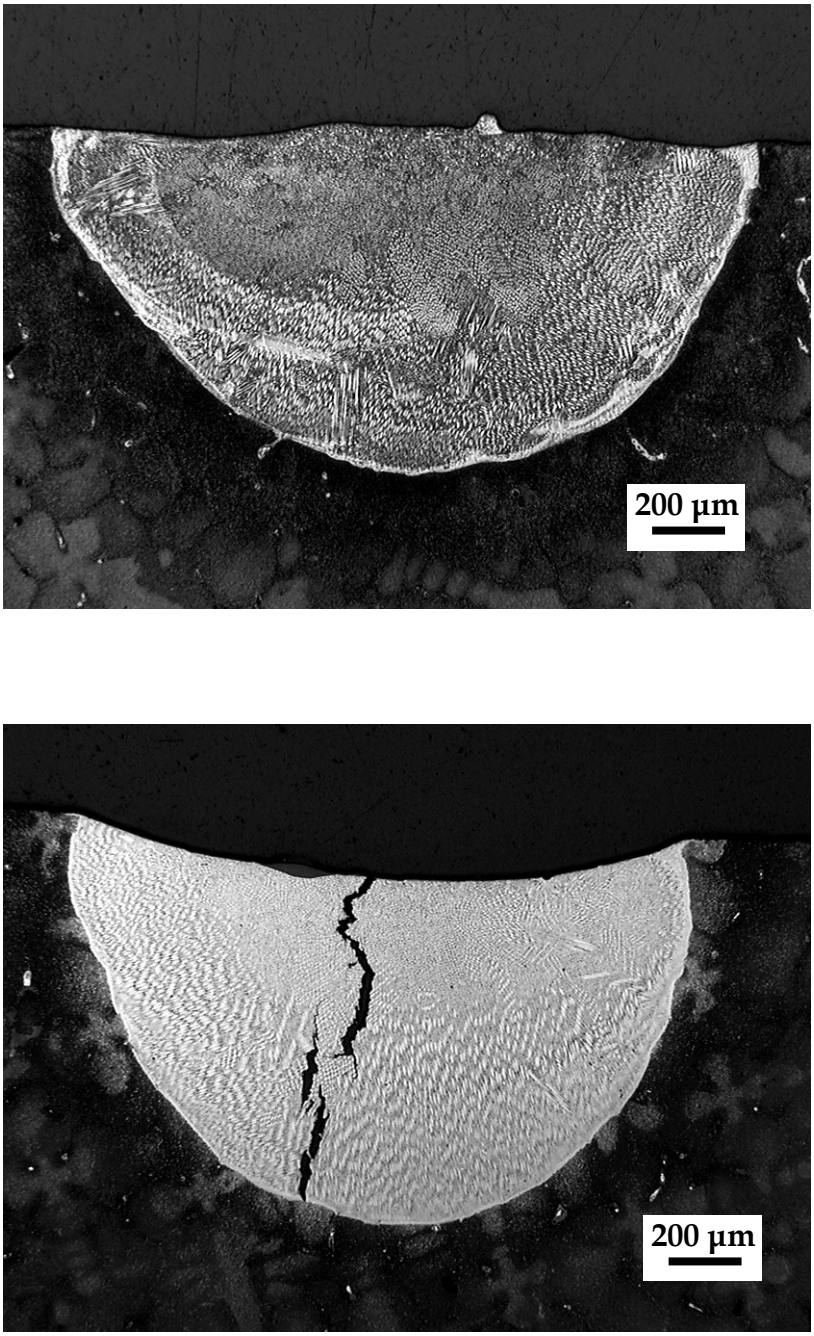

Figure 2: Laser welds using powder filler metal made on single-crystal Rene N5 base metal. (Top) weld with IN625 filler metal (no gamma prime second phase) and (bottom) weld with MarM247 filler metal (modest gamma prime content). Both welds show considerable stray-grain formation, but only the bottom weld showed cracking along stray-grain boundaries.

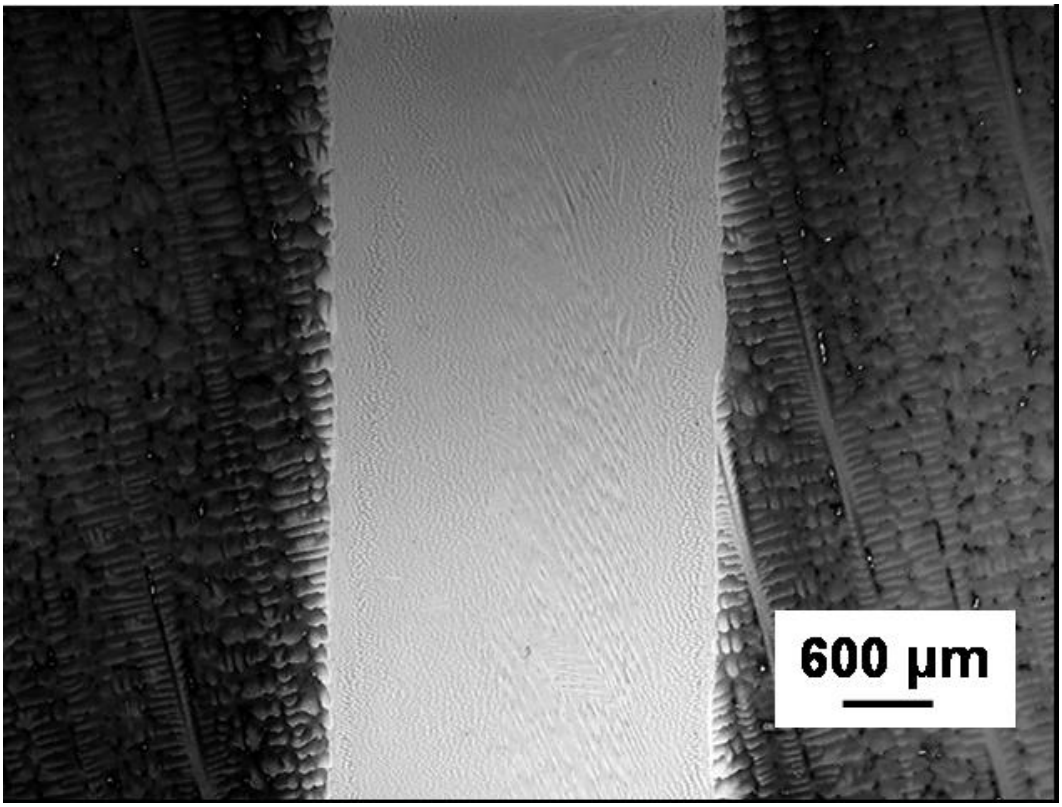

Figure 3: Low-speed (4.2 mm/s) and low-power (420 W) autogenous laser weld made on single-crystal Rene N5 alloy. Some stray grains are present, but no cracking was observed.

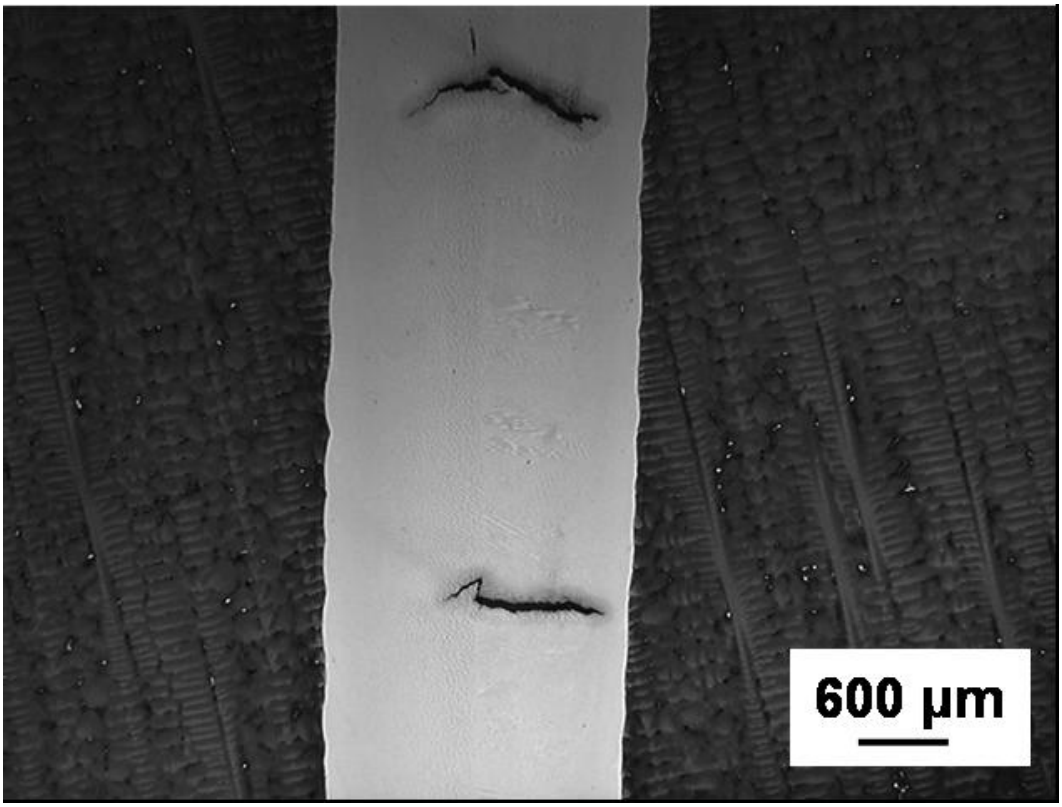

Figure 4: High-speed (21.2 mm/s) and high-power (840 W) autogenous laser weld made on single-crystal Rene N5 alloy. Stray-grain formation is extensive (see Figure 5) and cracking was observed, but preferentially along one side of the weld.

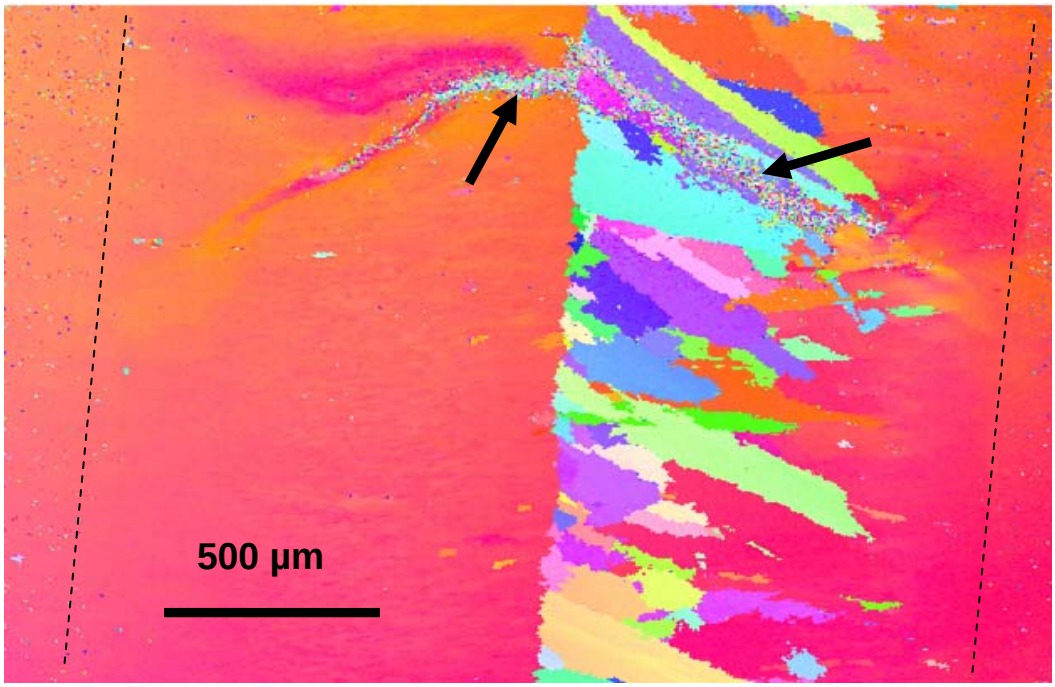

Figure 5: OIM image of high-speed, high-power weld (same weld as shown in Figure 4). Each color corresponds to a different crystallographic orientation. To the right of the weld centerline, extensive stray-grain formation is apparent. Arrows point to mottled feature, which corresponds to a crack and is seen to follow along the stray-grain boundaries.

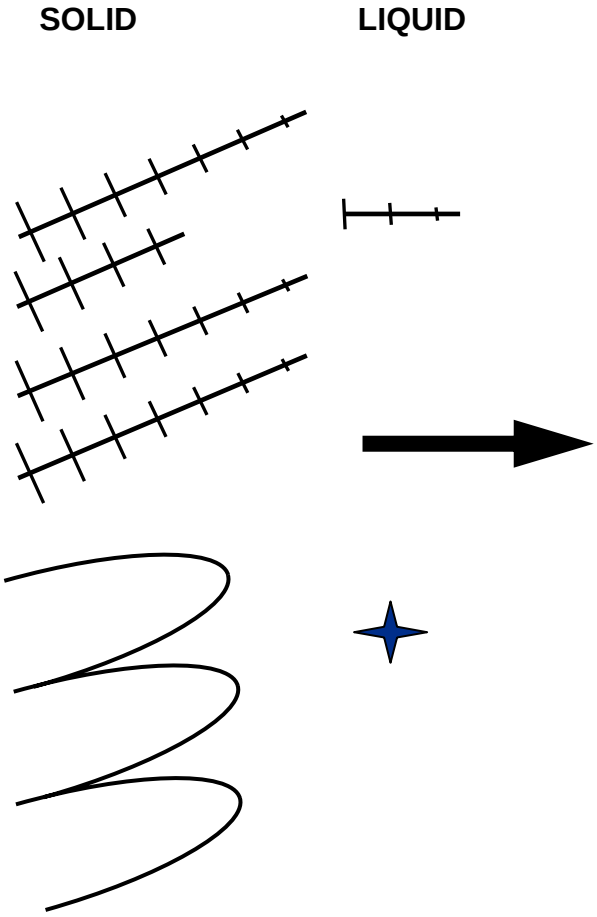

Figure 6: Schematic diagram showing the two possible mechanisms for stray-grain formation. Solidification is from left to right. In the fragmentation mechanism (top), dendrite tips may break off and act as new solidification sites. In the constitutional supercooling mechanism (bottom), new grains may form ahead of the advancing front in the supercooled liquid. In both mechanisms, new grains form most easily when the advancing solidification front is not well aligned with the thermal gradient (large arrow), as shown in the diagram.

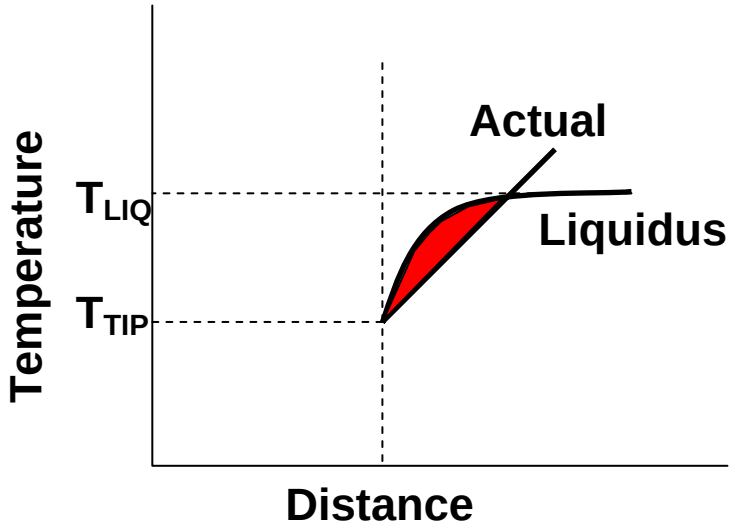

Figure 7: Schematic diagram showing the variation in actual temperature (line marked "Actual") and liquidus temperature (line marked "Liquidus") ahead of the advancing dendrite tip. The dendrite tip position is marked by the dashed vertical line. The dendrite tip temperature is T_{TIP} and the liquidus temperature for the overall alloy composition is T_{LIQ}. If the gradient is not sufficiently large, a supercooled region (shaded in red) exists in front of the dendrite tip.

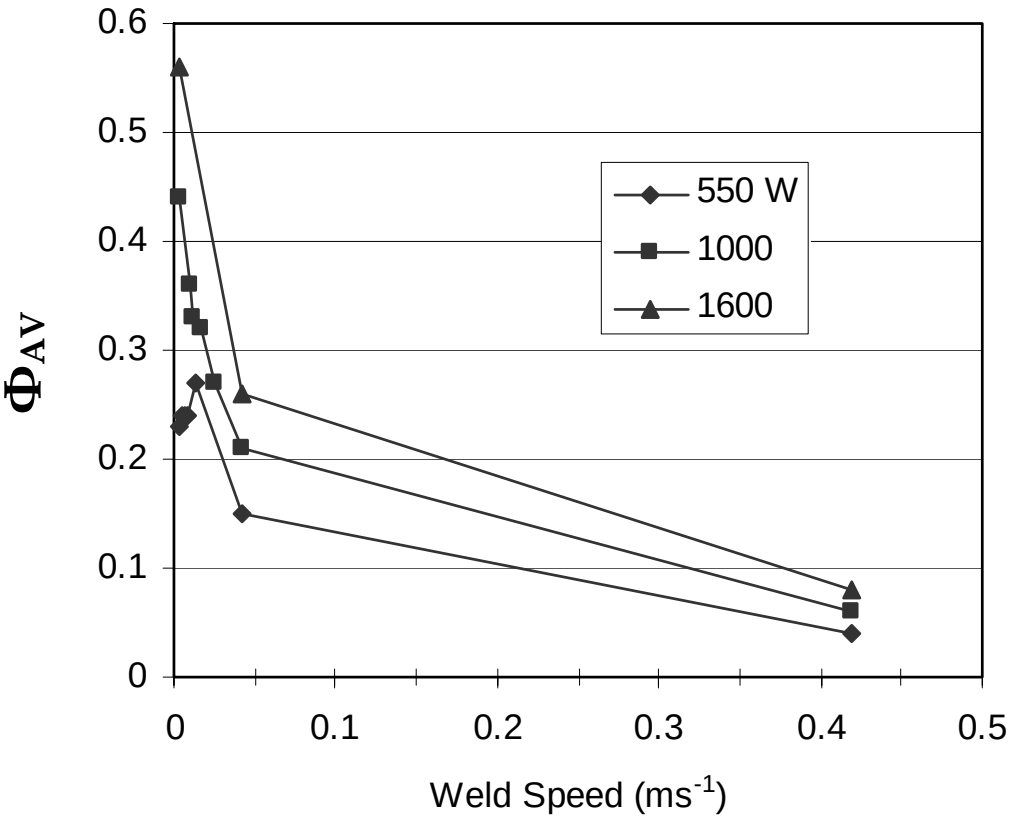

Figure 8: Calculated fraction of stray grains averaged over entire weld pool (Φ_{AV}) versus weld speed for three fixed weld powers.

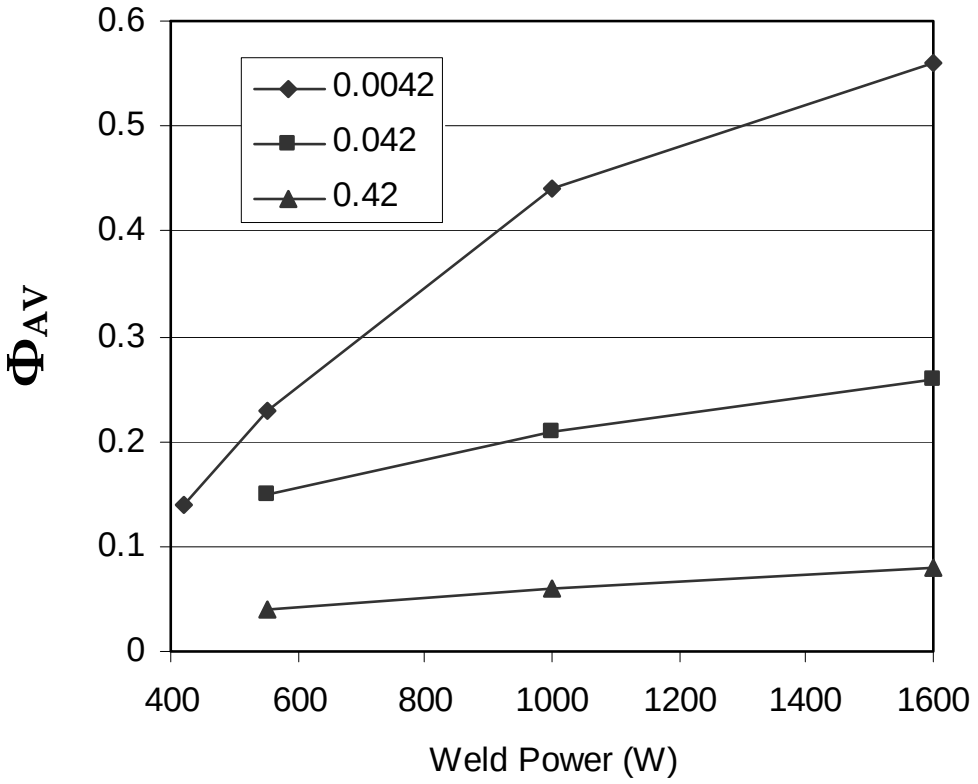

Figure 9: Calculated fraction of stray grains averaged over entire weld pool (Φ_{AV}) versus weld power for three fixed weld speeds.

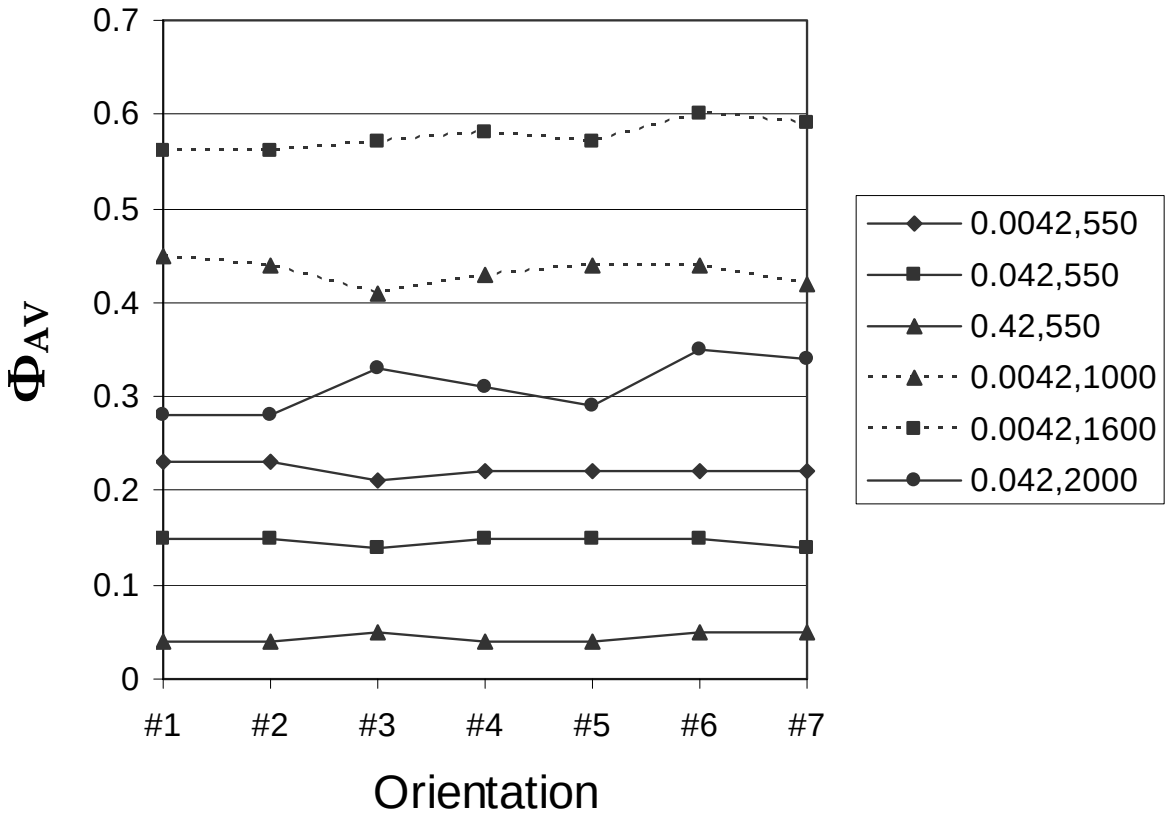

Figure 10: Calculated fraction of stray grains averaged over entire weld pool (Φ_{AV}) for seven different weld crystallographic orientations. Results are shown for six different combinations of weld speed (m/s) and weld power (W), with each symbol representing a different weld condition, as indicated. The stray-grain formation behavior is essentially independent of crystallographic orientation.

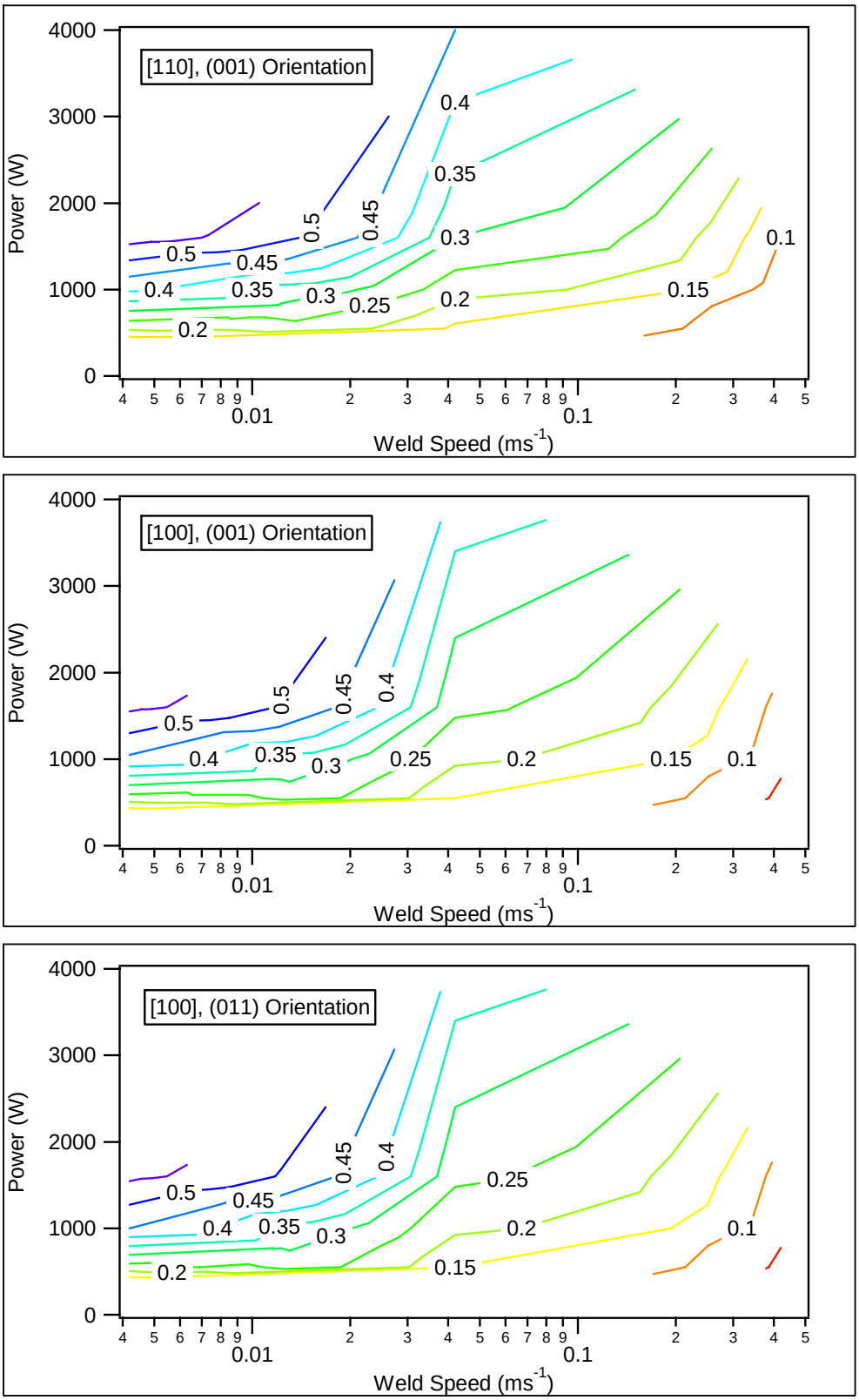

Figure 11: Contour plots of Φ_{AV} versus weld power and speed for three different weld orientations. High weld speed and low weld power lead to lowest values of Φ_{AV} .

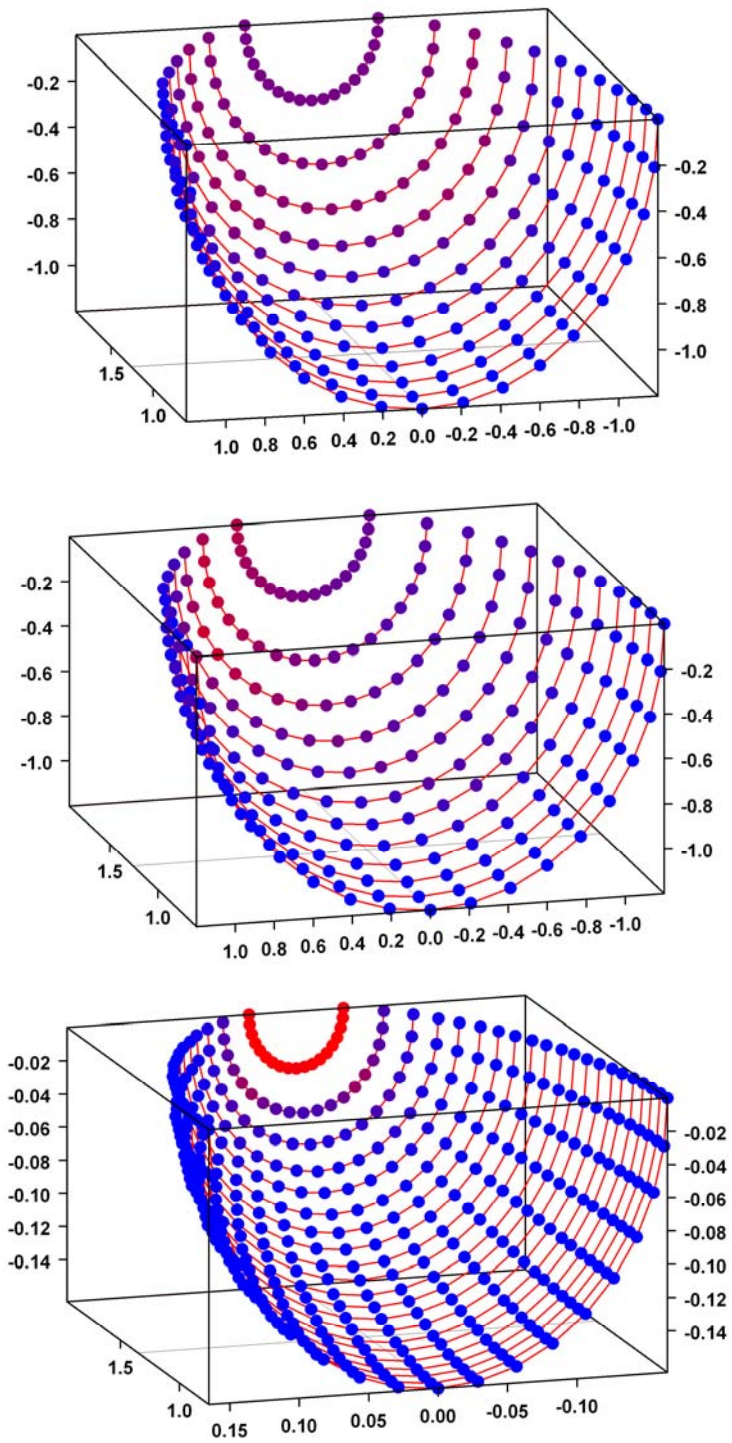

Figure 12: 3D views of calculated weld pool shapes, with values of Φ as a function of position superimposed (Φ = 0 = pure blue, Φ = 1 = pure red). The three conditions are: (top) low speed, low power, [100] weld direction, (010) weld surface; (middle) low speed, low power, [310] and (1 -3 7); and (bottom) high speed, low power, [100] and (010). Note that the purest red (highest Φ) is for the bottom condition but is limited to a small zone, and Φ is not symmetrical in the middle. Also note that the length scales are distorted; pool at bottom is considerably longer than other two weld pools.